12

Reliable and Repeatable Power Measurements in DVB-T Systems

Leopoldo Angrisani[1], Domenico Capriglione[2],
Luigi Ferrigno[2] and Gianfranco Miele[2]
[1]Dept. of Computer Science and Control Systems, University of Naples Federico II
via Claudio 21, 80125 Napoli,
[2]Dept. of Automation, Electromagnetism, Information Engineering and Industrial Mathematics, University of Cassino,
via G. Di Biasio, 43 03043 Cassino (Fr),
Italy

1. Introduction

Development and diffusion of digital video broadcasting (DVB) standards have revolutionized the television transmission; whether via satellite (DVB–S), via cable (DVB–C), or terrestrial (DVB–T), the number of services it can offer is able to satisfy the expectation of more demanding customers (ETSI, 2004), (Fischer, 2004). Since many countries in the world suffer from poor coverage of satellite and cable TV, DVB–T is playing a more significant role with respect to the other standards. DVB–T broadcasting networks are, in fact, growing very rapidly. A consequent and pressing need of performance assessment and large scale monitoring of DVB–T systems and apparatuses is thus posed. To reach this goal, a new set of measurements is required and a large number of parameters has to be taken into account, especially due to the complexity characterizing the DVB–T modulation process.
European Telecommunications Standards Institute (ETSI) specifies the parameters and quantities to be measured, and recommends the procedures to be adopted as well as test beds and laboratory equipments to be arranged (ETSI, 2004-2). Power measurement is, in particular, of primary concern: radiofrequency (RF) and intermediate frequency (IF) signal power, noise power, RF and IF power spectrum, should be measured as accurately as possible. Many advantages are connected with this practice, such as better optimization of transmitted power level, thus avoiding waste of energy and reducing the probability of interference with other systems that operate in the same coverage area, and reliable estimation of radiated emissions for verifying compliance limits applied in the regions of interest. Moreover, ETSI suggests the type of instrument to be used for power measurement, such as spectrum analyzer or power meter equipped with a proper sensor and a band-pass filter suitably tuned to the DVB–T frequency band. The former has to be equipped with a specific personality addressed to the integration of the input signal power spectrum on a certain frequency range (channel power measurement), the latter allows only peak and average power to be measured.
Several types of spectrum analyzer and power meter are available on the market. Most of them are general-purpose instruments, and not specifically designed to analyze DVB–T

Source: Digital Video, Book edited by: Floriano De Rango,
ISBN 978-953-7619-70-1, pp. 500, February 2010, INTECH, Croatia, downloaded from SCIYO.COM

signals. They exhibit relevant accuracy and repeatability problems in the presence of noise–like signals characterized by high peak to average power ratio (PAR), like DVB–T signals. In addition, they are not suited for large scale monitoring of DVB–T networks, where small size, light weight and low cost are critical constraints.
To give an answer to the cited needs, the scientific community has focused the attention on the definition and implementation of new digital signal processing (DSP) based methods for power measurement in DVB–T systems (Angrisani et al., 2006), (Angrisani et al., 2007), (Angrisani et al., 2008), (Angrisani et al., 2009). In particular, the methods based on power spectral density (PSD) estimators have seemed to be the most appropriate. They exploit straightforward measurement algorithms working on the achieved PSD to provide the desired value of the parameter or quantity of interest. Both non-parametric and parametric estimation algorithms have been considered. An overview of their performance in terms of metrological features, computational burden and memory needs if implemented on a real DSP hardware architecture is given hereinafter.

2. Power measurement in DVB-T systems

For assessing the performance of DVB-T systems and apparatuses, a new set of measurements is required. Many parameters and quantities have, in fact, to be evaluated, pointed out by ETSI in the ETSI TR 101 290 technical report (ETSI, 2004-2), called Digital Video Broadcasting Measurements (DVB-M). ETSI also recommends the procedures to be adopted for arranging test-beds or measurement systems.
A list of the measurement parameters and quantities defined for the DVB-T OFDM environment is shown in Table 1, and full referenced in (ETSI, 2004-2). All of them are keys for evaluating the correct operation of DVB-T systems and apparatuses, and each of them is addressed to a specific purpose. The technical report describes this purpose, where the parameter or the quantity has to be evaluated and in which manner. For the sake of clarity, it reports a schematic block diagram of a DVB-T transmitter and receiver, in which all the measurement interfaces are marked with a letter.
As it can clearly be noted from Table 1, power measurement is of great concern. RF and intermediate frequency (IF) signal power, noise power as well as RF and IF power spectrum are, in fact, relevant quantities to be measured as accurately as possible.
There are several RF power measurement instruments available in the market. They can be divided in two main categories: power meters and spectrum analyzers. Even though suggested by (ETSI, 2004-2), all of them suffer from a number of problems when measuring the power of a noise−like signal with a high PAR, as the DVB-T signal. The problems may dramatically worsen if the measurement is carried out in the field and with the aim of a large scale monitoring.
With regard to power meters, they are typically wideband instruments, and as such they must be connected to one or more calibrated band-pass filters centered at the central frequency of the DVB-T signals to be measured and with an appropriate bandwidth. Moreover, their metrological performance strongly depends on the power sensor they rely on. Several power sensors designed to measure different parameters and characterized by different frequency ranges are available on the market. Even though the choice is wide, not all power sensors are suitable to operate with signals characterized by a high PAR, as explained in (Agilent, 2003).

Measurement parameter	*T*	*N*	*R*
RF frequency accuracy (precision)	X		
Selectivity			X
AFC capture range			X
Phase noise of local oscillators	X		X
RF/IF signal power	X		X
Noise power			X
RF and IF spectrum	X		
Receiver sensitivity/ dynamic range for a Gaussian channel			X
Equivalent Noise Degradation (END)			X
Linearity characterization (shoulder attenuation)	X		
Power efficiency	X		
Coherent interferer			X
BER vs. C/N ratio by variation of transmitter power	X		X
BER vs. C/N ratio by variation of Gaussian noise power	X		X
BER before Viterbi (inner) decoder			X
BER before RS (outer) decoder			X
BER after RS (outer) decoder			X
I/Q analysis	X		X
Overall signal delay	X		
SFN synchronization		X	
Channel characteristics		X	

Table 1. DVB-T measurement parameters and their applicability

Differently from power meters, spectrum analyzers are narrowband instruments, and they are characterized by a more complex architecture. They allow different measurements on different RF signals. Their performance depends on several parameters like the resolution bandwidth (RBW), video bandwidth (VBW), detectors, etc. In particular, the detectors play a very important role because they can emphasize some signal characteristics giving unreliable measurement results. This is especially true when the signals involved are noise-like, as the DVB-T signal. To mitigate this problem, some suggestions described in (Agilent, 2003-2) can be followed.

In many cases, power meters and spectrum analyzers are expressly designed to be used only in laboratories; their performance drastically reduces when used in other environments, especially in the field. But, the fundamental problem that can limit their use is their cost. The total financial investment turns to be prohibitive for any interested company if a great number of instruments is needed, as when a large scale monitoring of DVB-T systems and apparatuses has to be pursued.

3. Nonparametric estimation for power measurement in DVB-T systems

In this chapter the most widely used correlation and spectrum estimation methods belonging to the nonparametric techniques, as well as their properties, are presented. They

do not assume a particular functional form, but allow the form of the estimator to be determined entirely by the data. These methods are based on the discrete-time Fourier transform of either the signal segment (direct approach) or its autocorrelation sequence (indirect approach). Since the choice of an inappropriate signal model will lead to erroneous results, the successful application of parametric techniques, without sufficient a priori information, is very difficult in practice. In the following two major nonparametric algorithms for PSD estimation have been taken into account (Angrisani L. et al., 2003). The first is based on the Welch method of averaged periodograms, which is also known as the WOSA estimator; the second applies wavelet thresholding techniques to the logarithm of the multitaper estimator.

3.1 WOSA Estimator

The WOSA estimator is computationally one of the most efficient methods of PSD estimation, particularly for long data records (Jokinen H. et al., 2000). This method is based on the division of the acquired signal x(n) into smaller units called segments, which may overlap or be disjoint. The samples in a segment are weighted through a window function to reduce undesirable effects related to spectral leakage. For each segment, a periodogram is calculated.

$$S_x^i(f) = \frac{T_S}{N_S U}\left|\sum_{n=0}^{N_S-1} x^i(n)\omega(n)e^{-j2\pi f n T_S}\right|^2 \tag{1}$$

Variable f stands for frequency, $x^i(n)$ are the samples of the i-th segment, $\omega(n)$ accounts for the window coefficients, N_S denotes the number of samples in a segment, U is a coefficient given by

$$U = \frac{1}{N_S}\sum_{n=0}^{N_S-1}\omega^2(n) \tag{2}$$

and is used to remove the window effect from the total signal power, and T_S represents the sampling period. The PSD estimate $S_x(f)$ is then computed by averaging the periodogram estimates

$$S_x(f) = \frac{1}{K}\sum_{i=0}^{K-1} S_x^i(f) \tag{3}$$

where K represents the number of segments and is given by

$$K = \frac{N - N_S}{N_S - N_P} + 1 \tag{4}$$

where N stands for the total number of acquired samples, and N_P is the number of the overlapped samples between two successive segments. Overlap ratio r is defined as the percentage of ratio between the number of the overlapped samples and the number of samples in a segment, i.e.,

$$r = 100\frac{N_P}{N_S}\%. \tag{5}$$

It is worth noting that proper use of the WOSA estimator imposes the optimal choice of two parameters: 1) window function $\omega(\cdot)$ and 2) overlap ratio r. The periodogram in (2) can be easily evaluated over a grid of equally spaced frequencies through a standard fast Fourier transform (FFT) algorithm (Welch P. D. 1967).

3.2 Multitaper estimation and wavelet thresholding

The idea is to calculate a certain number H of PSD estimates, each using a different window function, which is also called data taper and applied to the whole acquired signal, and then to average them together (Moulin P., 1994). If all data tapers are orthogonal, the resulting multitaper estimator can exhibit good performance, in terms of reduced bias and variance, particularly for signals characterized by a high dynamic range and/or rapid variations, such as those that are peculiar to DVB-T systems.
The multitaper estimator has the following form:

$$S_x(f) = \frac{1}{H}\sum_{i=0}^{H-1} S_x^i(f) \tag{6}$$

where the terms $S^i_x(f)$ called eigenspectra are given by

$$S_x^i(f) = \left|\sum_{n=0}^{N-1} x(n)h_i(n)e^{-j2\pi fnT_S}\right| \tag{7}$$

where $\{h_i(n) : n = 0,...,N-1; i=1,..., H\}$ denotes a set of orthonormal data tapers. A convenient set of easily computable orthonormal data tapers is the set of sine tapers, the i^{th} of which is

$$h_i(n) = \left(\frac{2}{N+1}\right)^{1/2} \sin\left(\frac{(i+1)\pi n}{N+1}\right). \tag{8}$$

A standard FFT algorithm proves to be appropriated in evaluating the eigenspectra over a grid of equally spaced frequencies (Walden et al., 1998).
Provided that H is equal to or greater than 5, it can be demonstrated that random variable $\eta(f)$, as given by

$$\eta(f) = \log\frac{S_x(f)}{S(f)} - \psi(H) + \log H \tag{9}$$

has Gaussian distribution with zero mean and variance σ^2_η equal to $\psi'(H)$; S(f) represents the true PSD, and $\psi(\cdot)$ and $\psi'(\cdot)$ denote the digamma and trigamma functions, respectively (Moulin P., 1994). If we let

$$Y(f) = \log S_x(f) - \psi(H) + \log H \tag{10}$$

we have

$$Y(f) = \log S(f) + \eta(f) \tag{11}$$

i.e., the logarithm of the multitaper estimator, plus a known constant, can be written as the true log spectrum plus approximately Gaussian noise with zero mean value and known variance σ^2_η.
These conditions make wavelet thresholding techniques particularly suitable to remove noise and, thus, to produce a smooth estimate of the logarithm of the PSD. In particular, after evaluating the discrete wavelet transform (DWT) of Y(f) computed according to (10), the resulting wavelet coefficients, which are also Gaussian distributed, can be subjected to a thresholding procedure, and the aforementioned smooth estimate can be obtained by applying the inverse DWT to the thresholded coefficients (Walden et al., 1998). A soft threshold function $\delta(\alpha,T)$ is suggested, and it is defined by

$$\delta(\alpha,T)=\mathrm{sgn}(\alpha)\begin{cases}|\alpha|-T, & \text{if } |\alpha|>T\\ 0, & \text{otherwise}\end{cases} \tag{12}$$

where α denotes the generic wavelet coefficient, and T is the threshold level. In (Donoho D. L. & Johnstone I. M., 1994), Donoho and Johnstone demonstrated that, in the presence of Gaussian noise with zero mean value and variance σ^2_η, the optimal value of T is

$$T=\sigma_\eta\sqrt{2\times\log N} \tag{13}$$

where N, which is the number of samples, must be of power of two.
In addition, in this case, the right choice of two parameters, i.e., the number of data tapers H and the mother wavelet $\zeta(\cdot)$ for DWT and inverse DWT evaluation, has to be made to gain a sound spectral estimation.

3.3 Performance optimization and assessment

To optimally choose window function $\omega(\cdot)$ and overlap ratio r for the WOSA estimator and the number of data tapers H and mother wavelet $\zeta(\cdot)$ for the multitaper estimator, a suitable simulation stage has been designed. Regarding r, all values ranging from 0% up to 90%, with a step of 10%, have been considered. As for $\omega(\cdot)$, a large set of functions, which differ from one another in relevant spectral characteristics, has been arranged; the set includes most windows defined in (Reljin I. et al., 1998), such as Hanning, Blackman, MS-3FT, MS-4FT, FD-3FT, and FD-4FT, and the new window proposed in (Jokinen H. et al., 2000), which is referred to as Ollila. Concerning H, the considered values range from 5 up to 50, with a step of 5. In addition, various mother wavelets characterized by different vanishing moments (db3, db8, sym3, sym8, coif1, coif5, bior2.2, and bior2.8) have been enlisted (Daubechies I., 1992).
A number of numerical tests have, in particular, been executed in the Matlab 7 environment, with the aim of minimizing the following figures of merit:

1. experimental standard deviation characterizing both total (σ_T) and channel (σ_C) power measurement results;
2. difference between the mean value of the results provided by the method and the imposed value, which is considered as reference, for both total (Δ_T) and channel (Δ_C) power.

The channel power is obtained by integrating the PSD over the frequency interval that is centered at the tune frequency and as wide as the nominal spacing of the channel itself

(ETSI, 2004). Instead the total power is evaluated integrating the PSD over the whole frequency span analyzed from zero up to half of the adopted sample rate f_S ($f_S=1/T_s$).
DVB-T reference signals have first been generated. To this aim, the analytical expression for the PSD of a DVB-T signal given by

$$S_X(f) = \sum_{k=-(K-1)/2}^{(K-1)/2} \left[\frac{\sin\left(\pi(f - f_k)(\Delta + T_u)\right)}{\pi(f - f_k)(\Delta + T_u)} \right]^2 \quad f_k = f_c + \frac{k}{T_u} \tag{14}$$

has been considered, where f_c is the RF signal central frequency, K is the number of transmitted carriers, Δ is the duration of the guard interval, and T_u is the time duration of the useful part of a DVB-T symbol (the useful part does not include the guard interval) (ETSI, 2004). Moreover, the approximate method in the frequency domain presented in (Percival D. B., 1992) has been adopted. It assures accurate time-domain realizations of a zero-mean Gaussian process, which is characterized by a known PSD.
The following DVB-T transmission settings have been imposed: 8K transmission mode (K=6817 and T_u=896 μs) and 1/4 (Δ=224 μs) and 1/32 (Δ=28 μs) guard intervals. In addition, three values of the oversampling factor (considered as the ratio between the sample rate and the RF signal central frequency) have been simulated, and the hypothesis of the acquired records covering one DVB-T symbol has been held. For each transmission setting and oversampling factor value, 50 different realizations (test signals) have been produced.
The obtained results are given in Tables 2 and 3 for the multitaper and WOSA estimators, respectively. Each pair of round brackets describes the couple ($\zeta(\cdot)$ − H or $\omega(\cdot)$ − r) that minimizes the related figure of merit. The last row of both tables quantifies the computation burden in terms of mean processing time on a common Pentium IV computer.
From the analysis of the results, some considerations can be drawn.

- Both estimators have assured good repeatability; the experimental standard deviation is always lower than 0.20%.
- Repeatability improves upon the widening of the guard interval, and the oversampling factor seems to have no influence.
- The WOSA estimator exhibits better performance in terms of Δ_T and Δ_C.
- Measurement time peculiar to the multitaper estimator is much longer than that taken by the WOSA estimator.

The WOSA estimator has given a better trade-off between metrological performance and measurement time, thus confirming the outcomes presented in (Angrisani L. et al., 2006). This is the reason the multitaper estimator has no longer been considered in the subsequent stages of the work.
To fix the minimum hardware requirements of the data acquisition system (DAS) to be adopted in the experiments on emulated and actual DVB-T signals described in the succeeding sections, further tests have been carried out. The sensitivity of the proposed method to the effective number of bits (ENOB) and acquired record length has been assessed. The obtained results are given in Figs. 1 and 2; they refer to a guard interval equal to 224 μs. In particular, Fig. 1 shows the values of σ_C [Fig. 1(a)], Δ_C [Fig. 1(b)], and Δ_T [Fig. 1(c)] versus ENOB for three values of the oversampling factor; Fig. 1(d) presents the estimated PSD for the considered values of ENOB. With regard to σ_T , values very similar to those characterizing σ_C have been experienced. Fig. 2 shows the values of σ_T [Fig. 2(a)] and Δ_T [Fig. 2(b)] versus the acquired record length for the same values of the oversampling factor. With regard to σ_C and Δ_C, values very similar to those characterizing σ_T and Δ_T, respectively, have been experienced.

		Oversampling factor		
Figure of merit	Guard interval [μs]	~3	~6	~12
σ_T [%]	28	0,148 (sym8,10)	0,176 (db3,25)	0,151 (db3,25)
	224	0,129 (coif1,50)	0,097 (coif1,50)	0,117 (db3,25)
σ_C [%]	28	0,148 (sym8,10)	0,176 (db3,25)	0,151 (db3,25)
	224	0,129 (coif1,50)	0,097 (coif1,50)	0,117 (db3,25)
Δ_T [%]	28	0,1104 (bior2.8,50)	0,1252 (bior2.8,50)	0,6335 (bior2.8,50)
	224	0,1509 (bior2.8,50)	0,1050 (bior2.8,50)	0,1237 (bior2.8,50)
Δ_C [%]	28	0,1105 (bior2.8,50)	0,1253 (bior2.8,50)	0,6336 (bior2.8,50)
	224	0,1509 (bior2.8,50)	0,1050 (bior2.8,50)	0,1238 (bior2.8,50)
Measurement time [s]	28	12,55	59,46	280,53
	224	53,61	280,58	1168,20

Table 2. Results obtained in the simulation stage: multitaper estimator is involved.

		Oversampling factor		
Figure of merit	Guard interval [μs]	~3	~6	~12
σ_T [%]	28	0,149 (Ollila,70)	0.181 (Ollila,50)	0,148 (Ollila,30)
	224	0,130 (blackman,60)	0,098 (hanning,50)	0,092 (Ollila,50)
σ_C [%]	28	0,149 (Ollila,70)	0,181 (Ollila,50)	0,148 (Ollila,30)
	224	0,130 (blackman,60)	0,098 (hanning,50)	0,092 (Ollila,50)
Δ_T [%]	28	0,0015 (FD3FT,30)	5,4091e-4 (FD3FT,30)	0,0017 (FD4FT,60)
	224	0,0068 (blackman,40)	0,0028 (MS3FT,10)	0,0020 (MS4FT,60)
Δ_C [%]	28	0,0015 (FD3FT,30)	6,0611e-4 (FD3FT,30)	0,0012 (FD4FT,60)
	224	0,0068 (blackman,40)	0,0017 (MS3FT,10)	0,0020 (MS4FT,60)
Measurement time [s]	28	0,032	0,052	0,096
	224	0,053	0,094	0,177

Table 3. Results obtained in the simulation stage: WOSA estimator is involved.

Looking at Fig. 1, it is possible to establish that 1) an ENOB equal to or greater than six grants an experimental standard deviation in both total (σ_T) and channel (σ_C) power measurements of less than 0.15%, and 2) Δ_C does not seem to be affected by vertical quantization, as, on the contrary, Δ_T does. Furthermore, Fig. 2 clearly evidences that σ_T improves upon the widening of the record length, whereas satisfying values of Δ_T can be achieved if the record lengths covering greater than one half of the DVB-T symbol are considered.

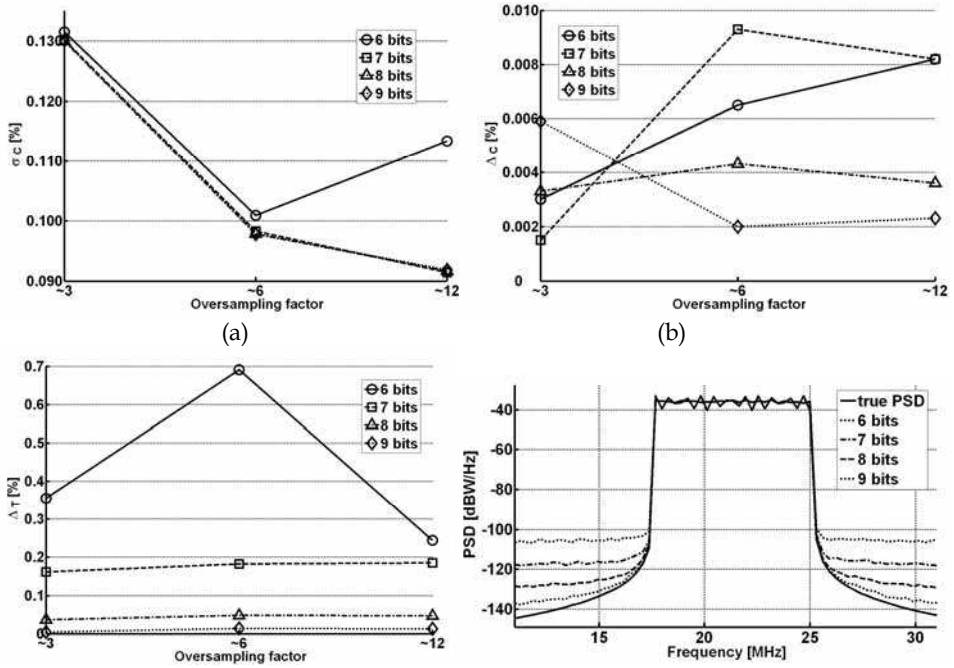

(a) (b) (c) (d)

Fig. 1. Simulation stage: a) σ_C, b) Δ_C, and c) Δ_T versus ENOB for three values of the oversampling factor; d) estimated PSD for the considered values of ENOB.

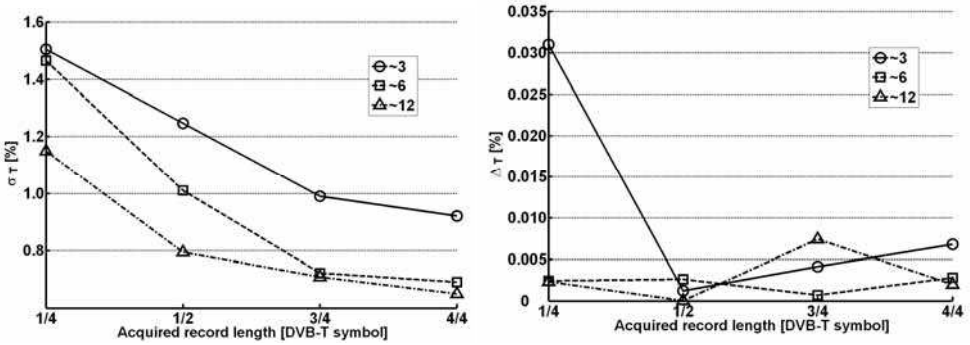

(a) (b)

Fig. 2. Simulation stage: a) σ_T and b) Δ_T versus acquired record length for three values of the oversampling factor.

These considerations match well with the typical characteristics of the data acquisition systems available on the market today. High values of the sample rate, required to optimally acquire RF or IF DVB-T signals, are often associated with ENOB not lower than 6 bits.
Further an emulation stage has been designed and applied, with the aim of assessing the performance of the proposed method in the presence of a real DAS and comparing it with that assured by competitive measurement solutions that are already available on the market. Stemming from past experience documented in (Angrisani L. et al., 2006), a suitable measurement station, which is sketched in Fig. 3, has been set up. It has included the following: 1) a processing and control unit, i.e., a personal computer, on which the measurement algorithm has run; 2) an RF signal generator equipped with DVB-T personalities Agilent Technologies E4438C (with an output frequency range of 250 kHz–6 GHz); 3) a traditional spectrum analyzer [express spectrum analyzer (ESA)] Agilent Technologies E4402B (with an input frequency range of 9 kHz–3 GHz); 4) a VSA Agilent Technologies E4406A (with an input frequency range of 7 MHz–4 GHz); 5) a real-time spectrum analyzer (RSA) Tektronix RSA3408A (with an input frequency range of dc–8 GHz); 6) an RF power meter (PM) Agilent Technologies N1911A equipped with two probes N1921A (with an input frequency range of 50 MHz–18 GHz) and E9304A (with an input frequency range of 6 kHz–6 GHz); and 7) a DAS LeCroy SDA6000A (with 6-GHz bandwidth and 20-GS/s maximum sample rate). They are all interconnected through an IEEE-488 interface bus. The function generator has provided 8-MHz-bandwidth DVB-T test signals characterized by an RF central frequency equal to 610 MHz, a nominal total power of -20 dBm, and a 64-state quadrature amplitude modulation (QAM) scheme. Moreover, the same transmission settings considered in the previous stage have been imposed.

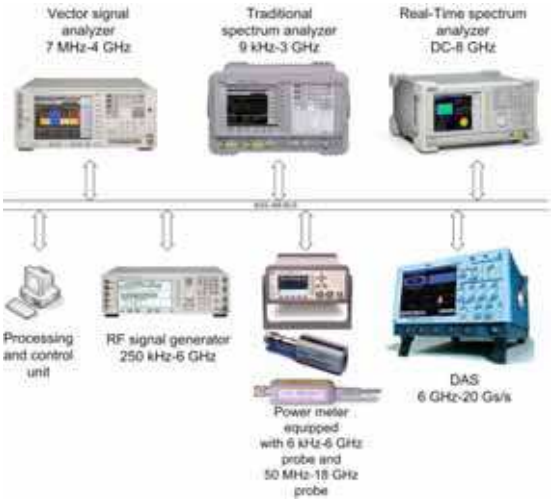

Fig. 3. Measurement station for performance assessment.

A preliminary characterization of cables and connectors utilized in the measurement station has been carried out through the vector network analyzer ANRITSU 37347C (with an input frequency range of 40 MHz–20 GHz), which is equipped with a 3650 SMA 3.5-mm calibration kit (Anritsu, 2003). The mean value and experimental standard deviation of 100 attenuation measures obtained in the interval of 606–614 MHz are given in Table 4.

	Mean attenuation	Experimental standard deviation
Power meter	0.829150	0.000039
Spectrum analyzers	0.834860	0.000019
Oscilloscope	0.834140	0.000014

Table 4. Characterization results of cables and connectors utilized in the measurement station of Fig. 3.

Different operative conditions of the DAS, in terms of vertical resolution (7 and 8 bits nominal) and observation period (1/4, 1/2, 3/4, and 1 DVB-T symbol), have been considered. For each operative condition and transmission setting, 50 sample records have been acquired and analyzed through the proposed method. Examining the obtained results given in Table 5 and Fig. 4, it can be noted that two conditions hold.

1. Higher sampling factors do not seem to affect the method's metrological performance; the same is true if vertical resolution is considered.
2. Performance enhancement can be noticed both in the presence of acquired records covering increasingly longer observation periods.

Successively, 50 repeated measurements of total and channel power have been executed by means of PM and spectrum analyzers (ESA, VSA, and RSA), respectively. Table 6 accounts for the results provided by the PM, whereas Table 7 enlists those that are peculiar to the analyzers. As an example, Fig. 5 sketches a typical PSD estimated by the proposed method [Fig. 5(a)], ESA [Fig. 5(b)], VSA [Fig. 5(c)], and RSA [Fig. 5(d)].

With regard to total power, three considerations can be drawn.

1. Results furnished by the PM are different for the two probes adopted.
2. Experimental standard deviation peculiar to the PM is slightly better than that assured by the proposed method.
3. PM outcomes concur with the total power measurement results of the proposed method; a confidence level equal to 99% is considered (Agilent, 2005).

As for the channel power, it is worth stressing that two conditions hold.

1. The proposed method exhibits satisfying repeatability. The related experimental standard deviation is better than that characterizing ESA, VSA, and RSA results.

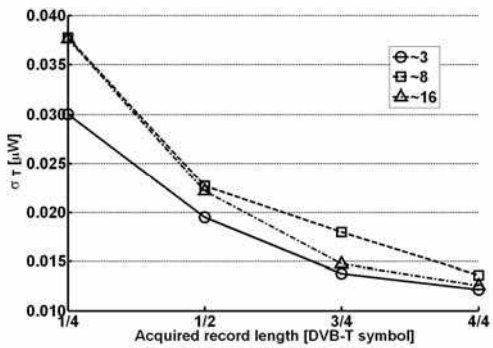

Fig. 4. Emulation stage: σ_T versus acquired record length for three values of the oversampling factor.

8k transmission mode, 64-QAM modulation scheme, 8 bit vertical resolution				
		Oversampling factor		
Figure of Merit	Guard Interval [μs]	~3	~8	~16
σ_T [μW]	28	0.012	0.014	0.013
	224	0.0094	0.017	0.011
σ_C [μW]	28	0.012	0.014	0.013
	224	0.0094	0.017	0.011
P_T [μW]	28	9.931	10.024	9.937
	224	10.142	10.163	10.144
P_C [μW]	28	9.890	9.989	9.895
	224	10.1030	10.125	10.105
8k transmission mode, 64-QAM modulation scheme, 7 bit vertical resolution				
		Oversampling factor		
Figure of Merit	Guard Interval [μs]	~3	~8	~16
σ_T [μW]	28	0.011	0.034	0.014
	224	0.011	0.029	0.015
σ_C [μW]	28	0.011	0.032	0.014
	224	0.011	0.028	0.016
P_T [μW]	28	10.148	10.162	10.157
	224	10.079	10.098	10.097
P_C [μW]	28	9.971	9.985	9.980
	224	9.899	9.919	9.916

Table 5. Total and channel power measures provided by the proposed method. The acquired record covers a single DVB-T symbol.

Transmission Settings 8k, 64-QAM, 610 MHz central frequency			
PM	Guard Interval [μs]	P_{PM} [μW]	σ_{PM} [μW]
N1921A PROBE	28	9.9444	0.0018
	224	9.9630	0.0020
E9304A PROBE	28	8.0402	0.0060
	224	7.95910	0.00086

Table 6. Mean values (PPM) and experimental standard deviations (σPM) of total power measures provided by the PM equipped with N1921A and E9304A probes.

2. ESA,VSA, and RSA outcomes concur with the channel power measurement results of the proposed method; a confidence level equal to 99% is considered (Agilent, 2004), (Agilent, 2001), (Tektronix, 2006).

Finally, a number of experiments on real DVB-T signals have been carried out through the optimized method. The signals have been radiated by two MEDIASET DVB-T multiplexers operating on the UHF 38 (610-MHz RF central frequency) and UHF 55 (746-MHz RF central frequency) channels, respectively.

A simplified measurement station, as sketched in Fig. 6, has been adopted. With respect to that used in the emulation stage, the function generator has been replaced by a suitable amplified antenna, the VSA and RSA have been removed, and a power splitter has been added. Cables, connectors, and a power splitter have been characterized through the

Transmission Settings: 8k, 64-QAM, 610 MHz central frequency					
Instrument		RBW [kHz]	Guard Interval [μs]	P_{SA} [μW]	σ_{SA} [μW]
ESA		100	28	10.322	0.074
		100	224	10.656	0.080
		30	28	10.376	0.068
		30	224	10.142	0.070
VSA		0.871	28	10.506	0.036
		0.871	224	10.218	0.023
		30	28	10.162	0.099
		30	224	9.52	0.12
RSA	SPECTRUM ANALYZERS	50	28	9.311	0.044
		50	224	9.318	0.042
		30	28	9.158	0.041
		30	224	9.042	0.044
	REAL TIME MODE		28	9.177	0.097
			224	9.088	0.081

Table 7. Mean values (P_{SA}) and experimental standard deviations (σ_{SA}) of channel power measures provided by ESA, VSA and RSA; different settings of their resolution bandwidth have been considered.

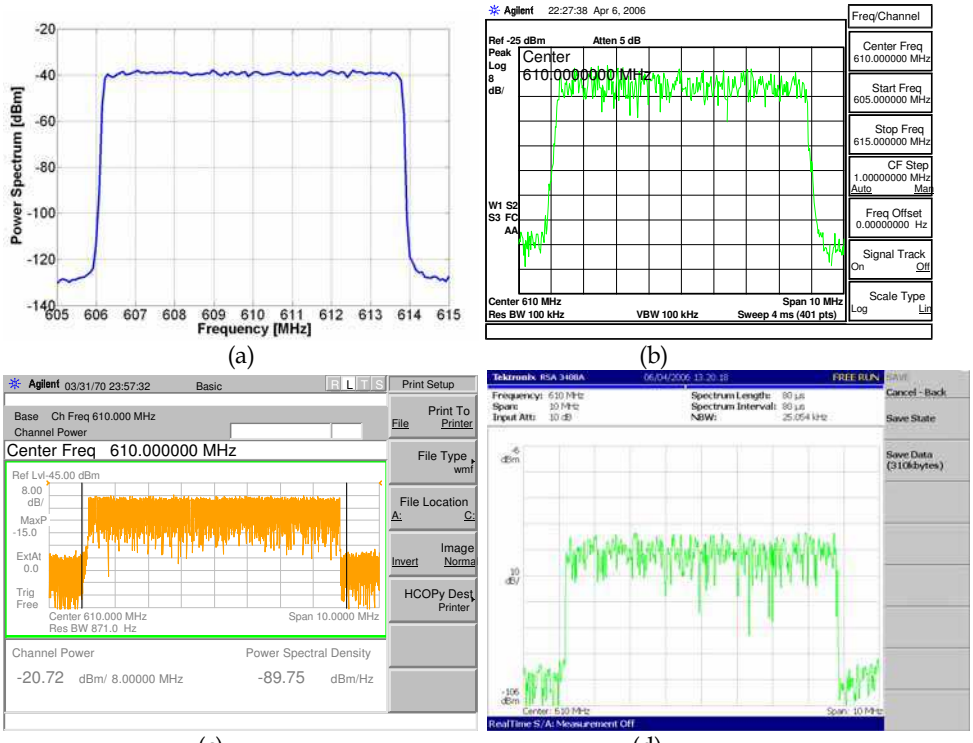

(a) (b)

(c) (d)

Fig. 5. Power spectrum of an emulated DVB T signal estimated by a) the proposed method, b) ESA, c) VSA and d) RSA.

aforementioned vector network analyzer. The mean value and experimental standard deviation of 100 attenuation measures obtained in the UHF 38 and UHF 55 channels are given in Table 8.

As an example, Fig. 7(a) and (b) shows the power spectrum of a DVB-T signal, which is radiated by the MEDIASET multiplexer operating on UHF 55, as estimated by the proposed method and ESA, respectively. Channel power measurement results are summarized in Table 9; good agreement can be appreciated, confirming the efficacy of the proposal (Angrisani L. et al., 2008).

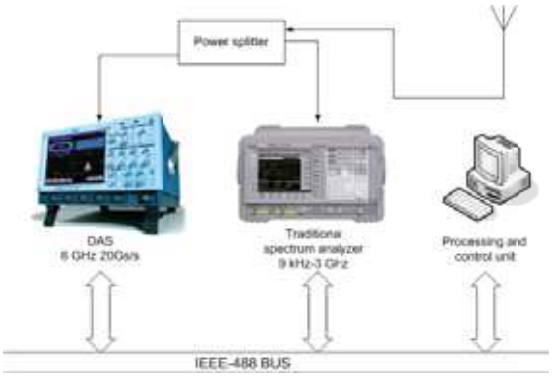

Fig. 6. Measurement station for the experiments on real DVB-T signals.

	UHF Channel	Mean attenuation [dB]	Experimental standard deviation [dB]
DAS	38	-4.703	0.032
	55	-5.403	0.042
Traditional Spectrum Analyzer	38	-19.393	0.021
	55	-19.3886	0.0086

Table 8. Characterization results of cables and connectors utilized in the measurement station of Fig. 6.

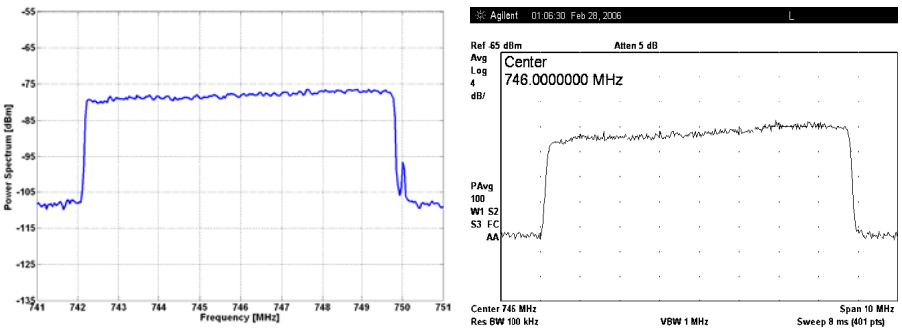

(a) (b)

Fig. 7. Power spectrum of a real DVB T signal measured by the a) proposed method and b) ESA.

8k transmission mode, 64-QAM, 28μs guard interval		
	UHF Channel 38 610 MHz	UHF Channel 55 746 MHz
Proposed Method	90.94 nW	93.07 nW
Traditional Spectrum Analyzer	94.06 nW	93.23 nW

Table 9. Experimental results.

4. Parametric estimation for power measurement in DVB-T systems

Parametric estimation methods suppose that the analyzed signal is the output of a model, which is represented as a linear system driven by a noise sequence ε_n. They evaluate the PSD of the signal by estimating the parameters (coefficients) of the linear system that hypothetically "generates" the signal. Among the various methods, autoregressive (AR) approaches are widespread. The computational burden related to AR approaches is, in fact, significantly less than that required to implement moving average (MA) or autoregressive moving average (ARMA) parameter estimation algorithms (Marple, 1980).
A stationary autoregressive process of order p, i.e., AR(p), satisfies

$$x_n = -\sum_{m=1}^{p} a_{p,m} x_{n-m} + \varepsilon_n \tag{15}$$

where $a_{p,1}$, $a_{p,2}$,..., $a_{p,p}$ are fixed coefficients, and $\{\varepsilon_n\}$ is a white noise process with variance σ^2_p. The PSD of the stationary process described by AR(p) is totally described by the model parameters and the variance of the white noise process. It is given by

$$S(f) = \frac{\sigma_p^2 T_S}{\left| 1 + \sum_{m=1}^{p} a_{p,m} e^{-j2\pi m f T_s} \right|^2} \quad |f| \le f_N \tag{16}$$

where $T_S = 1/f_S$ is the sampling interval, and $f_N = 1/(2T_S)$ is the Nyquist frequency.
Consequently, with known p, it is necessary to properly estimate the p+1 parameters $a_{p,1}$, $a_{p,2}$,..., $a_{p,p}$ and σ^2_p. To reach this goal, the relationship between the AR parameters and the autocorrelation sequence (known or estimated) of x_n has to be fixed, as described here.

4.1 Yule–Walker equations

Achieving the expectations on the product $x_n x^*_{n-k}$, the autocorrelation sequence is evaluated as

$$R_{xx}(k) = E\left[x_n x^*_{n-k}\right] = -\sum_{m=1}^{p} a_{p,m} R_{xx}(k-m) + E\left[\varepsilon_n x^*_{n-k}\right]. \tag{17}$$

The plausible fact that $E[\varepsilon_n x^*_{n-k}] = 0$, for $k > 0$, implies that

$$\begin{aligned} E\left[\varepsilon_n x_n^*\right] &= E\left[\varepsilon_n \left(-\sum_{m=1}^{p} a_{p,m}^* x_{n-m}^* + \varepsilon_n^* \right)\right] = \\ &= -\sum_{m=1}^{p} a_{p,m}^* E\left[\varepsilon_n x_{n-m}\right] + \sigma_p^2 = \sigma_p^2 \end{aligned} \tag{18}$$

Hence, the evaluation of (18) for k=0,1,...,p makes it possible to obtain the so-called augmented Yule–Walker equations

$$\overbrace{\begin{bmatrix} R_{xx}(0) & R_{xx}(-1) & L & R_{xx}(-p) \\ R_{xx}(1) & R_{xx}(0) & L & R_{xx}(-p+1) \\ M & M & O & M \\ R_{xx}(p) & R_{xx}(p-1) & L & R_{xx}(0) \end{bmatrix}}^{R_p} \overbrace{\begin{bmatrix} 1 \\ a_{p,1} \\ M \\ a_{p,p} \end{bmatrix}}^{A_p} = \overbrace{\begin{bmatrix} \sigma_p^2 \\ 0 \\ M \\ 0 \end{bmatrix}}^{\Sigma_p}. \tag{19}$$

If we have no stationary process $\{x_n\}$ but we are in the presence of a time series that is a realization of a portion $x_1, x_2, \ldots, x_N$ of any discrete-parameter stationary process, replacing $R_{xx}(k)$ with

$$\hat{R}_{xx}(k) = \frac{1}{N}\sum_{i=0}^{N-k} x_i x_{i+k}^* \qquad \text{for } k=0,\ldots,p \tag{20}$$

it is possible to solve system (19) by inversion.

4.2 Levinson–Durbin algorithm

To avoid the matrix inversion, which is a time-consuming task and is performed using Gaussian elimination, that requires operations of order p^3, which are denoted as $o(p^3)$, the system (19) can be solved through Levinson-Durbin recursions (Kay & Marple, 1981), (Marple, 1980), which require only $o(p^2)$ operations. The algorithm proceeds with recursively computing the AR parameters for order k from the AR parameters previously determined for order k−1.

In particular, the recursive algorithm is initialized by

$$a_{1,1} = -\frac{R_{xx}(1)}{R_{xx}(0)} \tag{21}$$

$$\sigma_1^2 = \left(1 - \left|a_{1,1}\right|^2\right) R_{xx}(0) \tag{22}$$

and the recursion for k = 2, 3,..., p is given by

$$a_{k,k} = -\frac{R_{xx}(k) + \sum_{m=1}^{k-1} a_{k-1,m} R_{xx}(k-m)}{\sigma_{k-1}^2} \tag{23}$$

$$a_{k,m} = a_{k-1,m} + a_{k,k} a_{k-1,k-m}^*, \qquad 1 \le m \le k-1 \tag{24}$$

$$\sigma_k^2 = \sigma_{k-1}^2 \left(1 - \left|a_{k,k}\right|^2\right) \tag{25}$$

where $a_{k,k}$ is the reflection coefficient (Kay & Marple, 1981).

This algorithm is useful when the correct model order is not known a priori since (21)–(25) can be used to successfully generate higher order models until the modeling error σ_k^2 is reduced to a desired value.

4.3 Forward linear prediction algorithm

In the literature, several least-squares estimation procedures that directly operate on the data to yield better AR parameter estimates can be found. These techniques often produce better AR spectra than that obtained with the Yule–Walker approach.

Assume that the sequence $x_0,..., x_{N-1}$ is used to find the p-th-order AR parameter estimates. The forward linear predictor is (Makhoul, 1975)

$$\hat{x}_n = -\sum_{k=1}^{p} a_{p,k} x_{n-k}. \tag{26}$$

It is possible now to define the forward linear prediction error

$$e_p(n) = x_n - \hat{x}_n = \sum_{k=0}^{p} a_{p,k} x_{n-k} \quad \text{for } p \le n \le N\text{-}1 \tag{27}$$

where $a_{p,0}=1$. Therefore, $e_p(n)$, for n=p to n=N−1, can be obtained by

$$\overbrace{\begin{bmatrix} e_p(p) \\ M \\ e_p(N-1) \end{bmatrix}}^{E} = \overbrace{\begin{bmatrix} x_p & L & x_0 \\ M & & M \\ x_{N-1} & L & x_{N-p-1} \end{bmatrix}}^{X_p} \overbrace{\begin{bmatrix} 1 \\ a_{p,1} \\ M \\ a_{p,p} \end{bmatrix}}^{A} \tag{28}$$

where X_p is an (N−p)x(p+1) Toeplitz matrix.

The approach followed to estimate $a_{p,k}$ consists of minimizing a sum of $e_p(n)$ called prediction error energy, i.e.,

$$SS_p = \sum_{n=p}^{N-1} \left| e_p(n) \right|^2 = \sum_{n=p}^{N-1} \left| \sum_{k=0}^{p} a_{p,k} x_{n-k} \right|^2 = E^H E. \tag{29}$$

Using an alternative description of the N−p error equation (28) such as

$$E = \overbrace{\begin{bmatrix} y & X \end{bmatrix}}^{X_p} \overbrace{\begin{bmatrix} 1 \\ a \end{bmatrix}}^{A} \tag{30}$$

where $y = [x_p,..., x_{N-1}]^T$, $a = [a_{p,1},..., a_{p,p}]^T$, and $X = \begin{bmatrix} x_{p-1} & L & x_0 \\ M & & M \\ x_{N-2} & L & x_{N-p-1} \end{bmatrix}$ the prediction error energy (29) may be expressed as

$$SS_p = E^H E = y^H y + y^H X a + a^H X^H y + a^H X^H X a. \tag{31}$$

To minimize SS_p, this term must be set to zero (Marple, 1987), i.e.,

$$X^H y + X^H X a = 0_p, \tag{32}$$